Journal of Materials Chemistry C

ROYAL SOCIETY OF CHEMISTRY

PAPER

View Article Online
View Journal | View Issue

Cite this: J. Mater. Chem. C, 2023, 11, 9628

Glass structure as a driver of polaronic conductivity in phosphate glasses containing MoO_3 and WO_3†

Sanja Renka,[a] Radha D. Banhatti,[b] Grégory Tricot,[c] Petr Kalenda,[d] Luka Pavić,[a] Petr Mošner,[d] Ladislav Koudelka[d] and Ana Šantić *[a]

Glasses containing transition metal (TM) oxides exhibit polaronic conductivity which, according to a well-accepted view, depends on the overall amount of TMO and the fraction of reduced TM ions. In this study we show that in phosphate glasses containing WO_3 and MoO_3, polaronic conductivity is entirely governed by the structural features of the glass network and cannot be correlated with these parameters. Tungsten glasses are found to exhibit six orders of magnitude higher conductivity than their molybdenum counterparts despite a significantly lower fraction of W^{5+} ions and the compositional change of DC conductivity is non-monotonic in both glass systems. We relate the former effect to the tendency of WO_6 units to aggregate by forming W–O–W–O–W bonds which facilitate polaronic transport, in contrast to MoO_6 and MoO_4 units which are prone to incorporate into a phosphate network uniformly thus failing to provide such fast conduction pathways. More interestingly, we show that the latter effect originates from the manner in which tungstate or molybdate units are mutually linked within the phosphate network: if they form chains with a sufficient number of flexible terminal oxygen bonds (lower TMO content) polaronic transport is facilitated whereas if they connect three-dimensionally, causing a reduction in the number of terminal oxygens (higher TMO content), conductivity is hindered. A detailed analysis of frequency-dependent conductivity and permittivity using the MIGRATION concept helps us understand the structural features that influence conductivity in these glasses and points out the importance of network connectivity in the propagation of polarons on long-range and localized scales.

Received 16th March 2023,
Accepted 1st June 2023

DOI: 10.1039/d3tc00954h

rsc.li/materials-c

1. Introduction

Interest in electronically conducting oxide glasses was initiated more than 60 years ago by an investigation by Denton *et al.* on the glass-forming characteristics and electrical properties of vanadate glasses.[1] Since then, many other oxide glass systems have been found to exhibit electronic conduction and studies on the mechanism of electronic transport in these materials have been reported extensively. Generally, electronic conduction is a characteristic of oxide glasses containing transition metal (TM) oxides such as V_2O_5, WO_3, MoO_3 and Fe_2O_3.[2–5] In these glasses, TM ions are present in more than one oxidation state and the conduction arises by the transfer of electrons from TM ions in a low oxidation state to the ones in a high oxidation state. In this process, the transferred electron becomes self-trapped in the potential well formed by the displacement of the surrounding atoms and, together with the atomic displacements that produce the well, forms a quasiparticle called a polaron. Accordingly, conductivity in glasses containing TM oxides is polaronic by nature and follows the small polaron hopping theory.[3] It has been widely accepted that the main factors that influence polaronic conductivity in oxide glasses are the amount of TM oxides, the fraction of TM ions in different oxidation states and the distance between TM ions.[5–9] While the amount of transition metal oxides is a matter of choice of stoichiometry and related glass-forming ability, the fraction of TM ions in different oxidation states depends on many parameters, including preparation conditions such as the melting time, temperature and atmosphere, types of raw materials, concentration of TM oxides and presence of other substances in the batch.[10–12]

[a] Division of Materials Chemistry, Ruđer Bošković Institute, Bijenička cesta 54, 10000 Zagreb, Croatia. E-mail: asantic@irb.hr
[b] Gisela Tech. Assz., Konrad-Adenauer-Ring 51, 69214 Eppelheim, Germany
[c] LASIRE UMR-CNRS 8516, Université de Lille, Sciences et Technologies, Villeneuve d'Ascq F-59655, Lille, France
[d] Department of General and Inorganic Chemistry, Faculty of Chemical Technology, University of Pardubice, 53210 Pardubice, Czech Republic

† Electronic supplementary information (ESI) available. See DOI: https://doi.org/10.1039/d3tc00954h

Among various families of polaronic oxide glasses, phosphate glasses containing WO_3 and MoO_3 are especially attractive due to their wide glass-forming composition range and desirable physiochemical properties. Incorporation of MoO_3 and WO_3 into the phosphate glass increases the electrical conductivity and improves the mechanical properties and chemical resistance against atmospheric moisture as well as thermal stability against devitrification.[12] These properties make them important in various domains of applications including optical, photochromic and electrochromic to those related to gas sensors and solid state batteries.[12,13]

The first systematic study of the electrical transport in binary phosphate glasses containing WO_3 and MoO_3 was reported by Mansingh *et al.*[14–17] The authors investigated glasses within a relatively narrow composition range, from 60 to 85 mol% of MoO_3[15] and 67 to 80 mol% of WO_3,[16] and proposed small polaron hopping as the conduction mechanism in both glass systems. Furthermore, Murawski *et al.*[5] re-examined the DC conductivity reported by Mansingh *et al.* in the framework of Mott's theory[2] and proposed that in WO_3–P_2O_5 glasses hopping of small polarons exhibits an adiabatic character. On the other hand, MoO_3–P_2O_5 glasses were reported to show non-adiabatic small polaron hopping[5] in which an electron may not always follow the lattice motions and miss many coincident events before making a hop. In a number of studies that followed, the focus was placed on the effects of addition of alkali oxides or additional TM oxides on electrical transport in molybdenum- and tungsten-phosphate glasses whilst polaronic conduction in *simple* binary MoO_3–P_2O_5 and WO_3–P_2O_5 glass systems was investigated only sporadically.[18–21] In our recent studies[22,23] on electrical transport in alkali/silver–zinc–phosphate glasses containing WO_3 and MoO_3, we have showed that a significantly higher conductivity of the $60WO_3$–$40P_2O_5$ (in mol%) glass in comparison to that of the $60MoO_3$–$40P_2O_5$ (in mol%) analogue is related to a high tendency of clustering of tungstate units in the phosphate network which provides easy conducting pathways for polaron transport. In the $60WO_3$–$40P_2O_5$ glass, high conductivity was achieved despite a low fraction of W^{5+}/W_{tot} ($< 2\%$) indicating that the glass structure plays a pivotal role in the transport of polarons.

Through this work, we aim to gain deep insights into the dynamics of polarons in these materials by a detailed structural and electrical characterization of binary $x MoO_3$-$(100-x)P_2O_5$ and $x WO_3$-$(100-x)P_2O_5$ glasses in a wider range of composition, x = 49–81 mol%, using various experimental methods (Raman, ^{31}P MAS-NMR, ESR and impedance spectroscopies) and numerical modelling of electrical conductivity and permittivity spectra using the MIGRATION concept.[24] The results reported in this work prove that the glass structure is a key factor for polaronic conductivity in these glasses. In particular, the structure can facilitate or hinder the transport of polarons depending on the manner in which the tungstate or molybdate units are linked. These findings deepen our understanding of the nature of polaron transport in binary oxide glasses and open possibilities for engineering desired compositions of highly electronically conducting tungsten- and molybdenum-phosphate materials.

2. Experimental and computational procedures

2.1 Experimental

Two binary glass series $x WO_3$-$(100-x)P_2O_5$ and $x MoO_3$-$(100-x)P_2O_5$, x = 49–81 mol%, were prepared by melt-quenching technique from reagent grade chemicals H_3PO_4 (85.0%, PENTA), WO_3 (99.9%, Sigma-Aldrich) and MoO_3 (99.9% Sigma-Aldrich) in batches of 25 g. Homogenized starting mixtures were slowly calcined up to 600 °C and held at that temperature for 2 hours in order to remove water. The reaction mixtures were then melted at 1300–1450 °C under ambient air, in an alumina crucible, after which the melts were transferred to a graphite mould preheated at $T < T_g$. Obtained dark blue glasses were cooled to room temperature and their amorphous character was checked by X-ray diffraction analysis. The exact glass composition was determined using an energy dispersive X-ray analyzer (EDS) by analyzing the surface and cross-section of the prepared samples. The glasses in this work were labelled according to their composition, for example, W-50 corresponds to the $50WO_3$–$50P_2O_5$ (mol%) glass composition.

The glass density, ρ, was determined using a helium gas pycnometer AccuPyc II 1340, while the glass transition temperature, T_g, was measured on bulk samples using a thermomechanical analyzer TMA 402 F3 (Netzsch). Measurements were carried out under an inert atmosphere of N_2 at a heating rate of 5 °C min^{-1}. From the obtained dilatometric curves, T_g was determined from the change in the slope of elongation *vs.* temperature.

The electron spin resonance (ESR) spectra of the samples were recorded at ambient temperature at an X-band ($\sim$9.5 GHz) using a spectrometer ESR 221 Magnettech. A microwave power of 10 mW, sufficiently below the saturation power, was used. The obtained ESR spectra were double integrated and experimental parameters were used to obtain comparable areas of all spectra. Using Mn^{2+} as a standard, the spin concentration was determined for all samples and the ratio of Mo^{5+}/Mo_{tot} and W^{5+}/W_{tot} was calculated.

The Raman spectra of glasses were recorded in the range of 1500–200 cm^{-1} on glassy bulk samples at room temperature using a DXR Raman spectrometer Thermo Scientific with a 532 nm solid-state (Nd:YAG) diode pumped laser. The complex shape of the Raman spectra was analysed using the least square fitting procedure assuming the Gaussian shape for all bands. The position and intensity of each component band were determined from the deconvoluted Raman spectra. To find the optimal fit, a minimum number of bands corresponding to the number of distinct features observed in the Raman spectra such as resolved maximum and well detectable shoulders was used. The structural units in the phosphate network were classified according to their connectivity by Q^n notation where n represents the number of bridging oxygen atoms per PO_4 tetrahedron (n = 0–3).

^{31}P MAS-NMR experiments were performed at 162.9 MHz using a 9.4 T AVANCE II Bruker spectrometer equipped with a 4-mm probehead operating at 12.5 kHz. Each spectrum was collected with a pulse length of 1.5 μs (corresponding to a π/6 flip angle), 8–16 transients and a recycle delay of 5–15 s allowing for quantitative measurements.

Impedance spectroscopy was used for measuring the conductivity spectra of glasses. The glass samples were prepared as ~1 mm thick discs and gold electrodes (6 mm in diameter) were sputtered on both sides of the samples using a sputter coater SC7620. Complex impedance was measured using an impedance analyzer (Novocontrol Alpha-AN Dielectric Spectrometer) in wide frequency (0.01 Hz–1 MHz) and temperature (from −90 °C to 240 °C) ranges. The temperature was controlled to an accuracy of ±0.2 °C.

2.2. Numerical modelling of the conductivity and permittivity spectra

The modelling of the conductivity and permittivity spectra was performed using the MIGRATION concept (an acronym for MIsmatch Generated Relaxation for the Accommodation and Transport of IONs),[24,25] which was developed for describing ion dynamics in disordered structures such as ionic glasses, fragile melts and salt-in-polymer electrolytes. This model is based on a simple picture of understanding the success of the forward hop of a central ion, made at $t = 0$ to an adjacent suitable site, in terms of a time-correlation factor, $W(t)$. Since such a hop induces a dipole moment, $g(t)$, and a corresponding dipole field in its neighborhood, the multi-particle relaxation of the neighborhood triggers the correlated forward–backward hops of the central ion. Thus, the success (through a single attempt or repeated attempts) of the hop of the central ion over time is dependent on its elementary hopping rate as well as on the strength of the dipole moment and decay of the dipole field, which in turn depends on the effective number of ions, $N(t)$, in the neighborhood still responding to the dipole field.

Recently, we have shown that both the model leitmotif and its formulation can be used to describe the conductivity spectra and hence understand the charge transport in polaronic glasses as well,[9] since the polarisation field caused by the hopping polaron is to first order a dipole field. Furthermore, as per the small polaron theory, since the electron is at all times relaxed in the potential well of its lattice distortion (resulting in an induced dipole moment) it can respond rapidly to the induced dipole field, provided it finds transition ions of the correct oxidation state in its immediate neighbourhood.

A detailed formulation of the model can also be found in ref. 9. Here, it suffices to state in brief the essential fact that the time correlation factor $W(t)$ is calculated by solving two coupled rate equations defining the time-dependent decay of both $W(t)$ and $g(t)$, and a related third equation describing the decay of the dipole field, and these equations are formulated using three model parameters. These equations are

$$-\frac{\dot{W}}{W} = -B\dot{g};\ -\frac{\dot{g}}{g} = \Gamma_0 W(t)N(t);\quad N(t) - N(\infty) = [Bg(t)]^{K-1} \tag{1}$$

When introduced in a suitable scaled notation,[26] the solution for $W_s(t_s)$ is uniquely defined in terms of the three model parameters B, K and $N(\infty)$ and the Fourier transform of it yields an unique master curve of the conductivity and permittivity spectra.[26] In particular, this master curve, generated using a correct choice of value for parameter K, $(1 < K < 3)$ yields an appropriate fit reproducing the shape of the experimental conductivity spectra for describing conductivity dispersion; the choice of parameter B helps in modelling the height of conductivity dispersion and a correct choice of parameter $N(\infty)$, which is a measure of the effective number of charge carriers in the neighbourhood which at long times are still unshielded from the initial polarization field caused by the hop of a central charge carrier, helps model the scaled permittivity plateau at low scaled frequencies on experimental permittivity isotherms.[25] In Section 1 of the ESI,† more details on modelling, the parameters, and their implications for the transport of charge carriers in various kinds of oxide glasses are given.

What makes modelling experimental spectra using the MIGRATION concept unique is that it yields quantitative information which can be correlated to factors influencing the charge carrier dynamics. For example, one can calculate the spatial extent of the localised diffusion of the charge carrier,[26] a material property of the glass. Since, as stated above, the local glass structure is especially relevant for understanding charge transport in polaronic glasses, a systematic modelling of conductivity and permittivity isotherms for a wide range of compositions of polaronic glasses has been performed for the very first time using the MIGRATION concept, to ascertain how important is the role played by the glass network structure in facilitating charge transport in any given series of glasses and for a given glass composition,[26] and to help deepen our understanding of the fundamental features of polaronic transport in binary oxide glasses.

3. Results and discussion

3.1. Glass composition, thermal properties and oxidation states of molybdenum and tungsten ions

All glasses from both series, $x\mathrm{WO_3}$-$(100-x)\mathrm{P_2O_5}$ and $x\mathrm{MoO_3}$-$(100-x)\mathrm{P_2O_5}$, x = 49–81 mol%, were found to be fully amorphous, except the W-81 glass where traces of crystallization were detected. The glass composition determined by EDS analysis and selected physical parameters of the samples are reported in Table 1. The EDS analysis shows that glass samples contain very small amounts of Al (<0.8 wt%) due to a slight dissolution of Al_2O_3 crucibles during melting, see Section S2 of the ESI.† However, such small amounts are not expected to have any influence on the structural and physical properties of glasses. From Table 1, it can be seen that the addition of MoO_3 and WO_3 to phosphate glasses results in a steady increase of the glass density, ρ, but causes non-monotonic changes in the glass transition temperature (T_g). While a linear increase in ρ is related to the replacement of phosphate ions with heavier molybdenum/tungsten ones, the non-linear trend of T_g reflects the changes in the cross-link density and strength of the chemical bonds with the incorporation of molybdate/tungstate units. The initial increase in T_g from 495 °C to 585 °C with an increasing MoO_3 content from 49 to 57 mol% is associated with the higher cross-link density between the molybdate and phosphate units.

Table 1 Composition and selected physical parameters for xWO$_3$-(100−x)P$_2$O$_5$ and xMoO$_3$-(100−x)P$_2$O$_5$, x = 49–81 mol% glass series

Glass	Composition determined by EDS (mol%)		O/P ratio	ρ (g cm^{-3}) ± 0.02	T_g (°C) ± 2	W^{5+}/W$_{tot}$ (%)
	WO$_3$	P$_2$O$_5$				
W-50	50	50	4.0	4.02	680	1.9
W-61	61	39	4.8	4.55	662	0.2
W-66	66	34	5.4	4.75	760	1.0
W-71	71	29	6.2	5.00	721	0.5
W-81[a]	81	19	8.9	5.68	735	0.5
	MoO$_3$	P$_2$O$_5$				Mo^{5+}/Mo$_{tot}$ (%)
Mo-49	49	51	3.9	3.02	495	26.5
Mo-57	57	43	4.5	3.17	585	22.8
Mo-61	61	39	4.8	3.24	505	15.5
Mo-70	70	30	6.0	3.32	431	3.4
Mo-80	80	20	8.5	3.57	382	0.5

[a] Partially crystallized sample.

However, with further MoO$_3$ addition, T_g decreases as a result of depolymerization of the phosphate glass network, see Section 3.2.1., and the effect of the replacement of stronger P–O bonds (599 kJ mol^{-1}) with weaker Mo–O bonds (502 kJ mol^{-1}) that reduces the mean bond strength in the glass structure.[27–29] Unlike in the MoO$_3$ series, the differences in T_g values in the WO$_3$ series are much smaller and vary within a span of 100 °C. These variations result from the competing effect of the replacement of the P–O bonds by the stronger W–O bonds (720 kJ mol^{-1})[27–29] and a decrease in the cross-link density due to the depolymerization of the phosphate network and the clustering of WO$_6$ octahedra, see Section 3.2.1. Since the former effect dominates the latter, T_g of WO$_3$ containing glasses shows a slight increase over the entire range of compositions. For the same reason, tungsten glasses exhibit higher T_g values (662–760 °C) and hence form a more thermally stable glass network in comparison to the molybdenum glasses (T_g = 382–585 °C).

The dominant oxidation states of TM ions in these glasses are Mo^{6+} and W^{6+}, with some small fractions of Mo^{5+} and W^{5+} ions, see Table 1 and Section 3 of the ESI.† The fractions of W^{5+}/W$_{tot}$ (%) were found to be very low and approximately constant (0.2–1.9%) for all samples. On the other hand, in the molybdenum series, the Mo^{5+}/Mo$_{tot}$ ratio decreases from 26.5% in the Mo-49 glass to 0.5% in the Mo-80 glass showing the strongest decrease from the Mo-61 sample to the Mo-70 sample. The higher values of Mo^{5+}/Mo$_{tot}$ originate from the stronger reduction tendency of molybdenum in comparison with tungsten ions in the melting process.[12]

3.2. Network structure in WO$_3$–P$_2$O$_5$ and MoO$_3$–P$_2$O$_5$ glasses

3.2.1. Raman spectroscopy. The Raman spectra of glasses from both series are shown in Fig. 1. The spectra are dominated by broad, overlapping peaks that are indicative of the amorphous structure and correspond to the metal–oxygen stretching bands. The Raman spectra of glasses with a lower WO$_3$ content

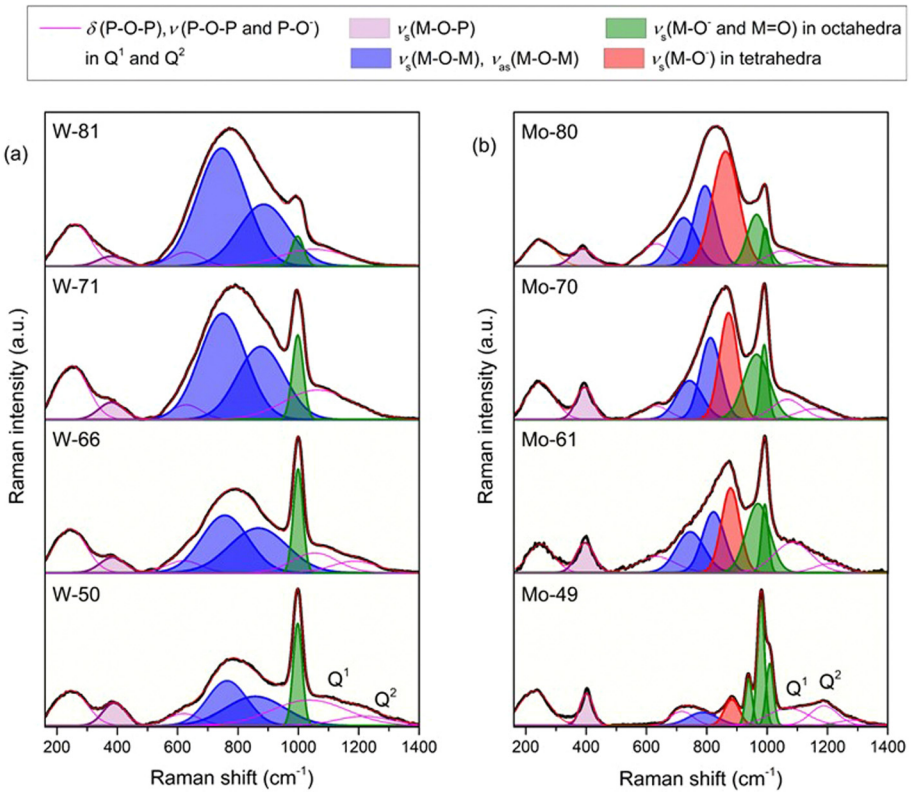

Fig. 1 Raman spectra of glasses from (a) xWO$_3$-(100−x)P$_2$O$_5$ and (b) xMoO$_3$-(100−x)P$_2$O$_5$, x = 49–81 mol%, series. The Raman spectra of W-61 and Mo-57 are similar to those of W-66 and Mo-61, respectively; hence, they are not shown.

($x \leq 66$ mol%) exhibit an intense band at $\approx$1000 cm^{-1} which corresponds to the stretching vibrations of terminal W=O and W–O$^-$ bonds in WO_6 octahedra, see Fig. 1(a).[27,30] These spectra also contain broad, less intense bands in the 750–880 cm^{-1} region, associated with the symmetrical and asymmetrical W–O stretching vibrations within W–O–W bonds.[27,30] With the increase in the WO_3 content, the intensity of the bands related to the vibrations of bridging oxygen in W–O–W bonds gradually increases, and for glasses with $\geq$71 mol% WO_3, these bands overpower the band associated with the vibrations of terminal oxygens. This indicates that WO_6 octahedra have a strong tendency to mutually interconnect and form a three-dimensional structural network. This is also supported by the fact that the band at $\approx$400 cm^{-1}, related to the stretching vibrations of P–O–W bonds,[22,23,27] decreases with the addition of WO_3 denoting a reduction in interconnectivity between WO_6 octahedra and phosphate units. Although the bands related to the phosphate units are of much smaller intensity and are greatly overlapped by the strong metal-oxygen bands, some conclusions can be drawn on their presence. That is, for glasses containing $\leq$66 mol% of WO_3, the relatively weak bands at $\approx$1080 cm^{-1} and $\approx$1210 cm^{-1} reveal that pyrophosphate (Q^1) and metaphosphate (Q^2) units are present in the glass network.[23] With an increasing WO_3 content above 66 mol%, only the band at $\approx$1080 cm^{-1} related to pyrophosphate units remains present indicating the complete depolymerization of metaphosphate chains. Here, it should be noted that the vibrations associated with the isolated orthophosphate (Q^0) units are completely covered by those of the tungsten-oxygen bands, so their presence is impossible to identify from the Raman spectra.

The evolution of the Raman spectra of phosphate glasses with the addition of MoO_3 shows somewhat different changes in the glass network, see Fig. 1(b). The most intense band at 980 cm^{-1} accompanied by a band at 939 cm^{-1} and a shoulder at 1012 cm^{-1} in the spectrum of the Mo-49 glass is ascribed to the stretching vibrations of terminal Mo–O$^-$ and Mo=O bonds in MoO_6 octahedra.[28,31] However, in this spectrum, there is an additional band at 883 cm^{-1} which is related to the stretching vibration of Mo–O$^-$ bonds in MoO_4 tetrahedra.[28,31] With an increasing MoO_3 content, the intensity of ν_s(Mo–O$^-$) in MoO_4 tetrahedra increases while that of ν_s(Mo–O$^-$) in octahedra decreases indicating the change in the coordination of molybdenum ions from six to four. Also, by comparing the spectra of both glass series, there is an obvious difference in the intensity of stretching bands of TM–O–TM and TM–O–P bonds. First, in tungsten containing glasses, ν(W–O–W) bands are strong throughout the whole series, whereas in MoO_3–P_2O_5 glasses, ν(Mo–O–Mo) bands are not so pronounced and their intensity does not increase so drastically. Second, the Raman band that corresponds to the stretching vibration of Mo–O–P bonds at $\approx$400 cm^{-1} is more pronounced than the equivalent band of W–O–P bonds and retains intensity throughout the glass series. These differences indicate that while in tungsten containing glasses WO_6 units mostly interconnect mutually, in molybdenum glasses molybdate units are more prone to associate with phosphate ones, thus forming a uniform phosphate–molybdate glass network.

However, along with the differences, there are also some similarities between the two glass series. In both systems, the increase in WO_3 and MoO_3 contents causes the depolymerization of metaphosphate chains and consequently the increase in the fraction of pyrophosphate units. But even more important is the fact that the Raman spectra of glasses containing less than 70 mol% of both WO_3 and MoO_3 (lower bright yellow panels in Fig. 1) are dominated by intense vibrations of terminal oxygen bonds, whereas for glasses with $\geq$70 mol% of WO_3 and MoO_3 (upper panels in Fig. 1) the bands related to bridging oxygens in W–O–W and Mo–O–Mo bonds prevail. The ratio between the terminal and bridging oxygen bonds will be shown to have surprisingly important implications for polaronic transport which is reported in the next sections.

3.2.2. ^{31}P MAS-NMR spectroscopy. The ^{31}P MAS-NMR spectra are reported in Fig. 2. All the experiments were performed

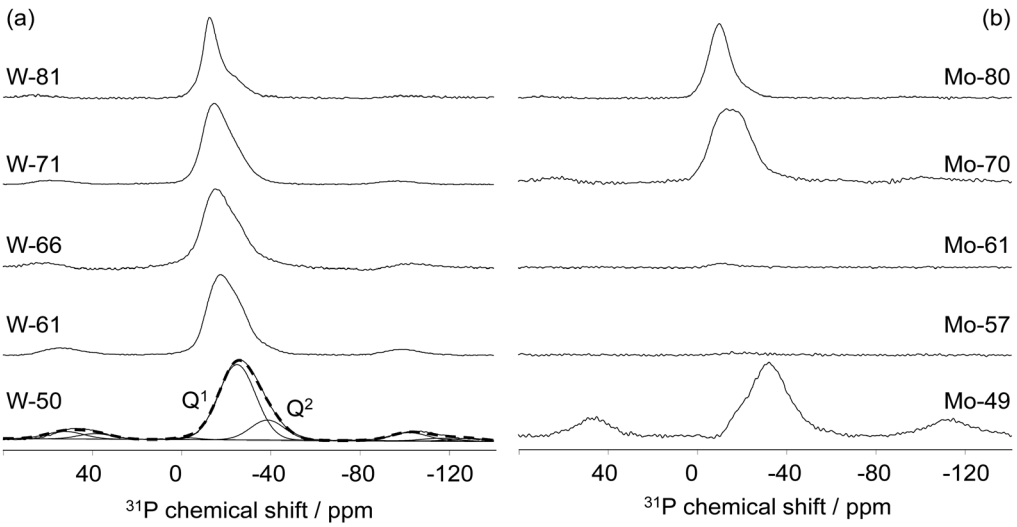

Fig. 2 ^{31}P MAS-NMR spectra of glasses from (a) $x$$WO_3$-(100−$x$)$P_2O_5$ and (b) $x$$MoO_3$-(100−$x$)$P_2O_5$, x = 49–81 mol%, series.

with very short recycle delays (5–15 s) compared to standard phosphate glasses (120–300 s) owing to the presence of W^{5+} and Mo^{5+} paramagnetic species. At very low amounts, the paramagnetic species decrease the relaxation time without disturbing the acquisition and the spectrum lineshape.[27] At higher amounts, the paramagnetic species significantly increase the peak broadness, resulting in a loss of signal. The analysis performed on the WO_3–P_2O_5 system are presented in Fig. 2(a). The spectra do not seem to be significantly disturbed by the paramagnetic species in line with the very low W^{5+}/W_{tot} values reported in Table 1. Two different signals can be observed for the W-50 samples at −24.7 and −36.6 ppm. Based on previous investigations,[31,32] these two signals were assigned to Q^1 and Q^2 species (where Q denotes the phosphate tetrahedron and n represents the number of connected P atoms), respectively. These two signals shift toward more positive values when the amount of WO_3 increases, suggesting that the phosphate network is depolymerized by the addition of tungsten oxide. The presence of these Q^2 and Q^1 sites is not expected because of the O/P ratio of 4. This ratio is usually associated with the presence of isolated Q^0 species. This difference can be explained by the presence of oxygens in the glass matrix that are not attached to any phosphorus atom. In the binary formulations studied here, these oxygens can only be associated with W–O–W bonds in line with the presence of clustered tungstate regions within the glass matrix. The ^{31}P MAS-NMR spectra of the MoO_3–P_2O_5 glasses are shown in Fig. 2(b). In this series, the paramagnetic effect of the Mo^{5+} ions on the ^{31}P NMR signal can be clearly observed, especially for the low MoO_3 content samples: Mo-49, Mo-57 and Mo-61. For the two letters, the Mo^{5+} paramagnetic effect causes a complete disappearance of the NMR signal suggesting that Mo^{5+} ions are completely distributed within the phosphate network. For the Mo-49 sample, the presence of the NMR signal suggests a longer distance between the paramagnetic ions and the P atoms than in the Mo-57 and Mo-61 compositions. No further analysis is allowed because of the low signal to noise ratio of the ^{31}P MAS-NMR spectra.

3.3. Polaronic transport in WO_3–P_2O_5 and MoO_3–P_2O_5 glasses

3.3.1. DC conductivity and parameters of the Austin–Mott equation. Fig. 3(a) shows the conductivity isotherms of Mo-61 glass as representative conductivity spectra for all studied glasses. Typically, the conductivity spectra of polaron conducting glasses exhibit two features. At lower frequencies, conductivity is frequency-independent and corresponds to the translational motions of polarons (DC conductivity) whereas at higher frequencies it increases with increasing frequency (conductivity dispersion) due to their correlated backward–forward hopping. With increasing temperature, the transition frequency between DC conductivity and dispersion shifts towards higher values and so, in the conductivity spectra, the DC conductivity mainly prevails at highest temperatures while dispersive behavior dominates at lowest temperatures. In the following, we analyze in detail both conductivity features, first by addressing the temperature and composition dependence of the DC conductivity and second by examining the dispersive part of the conductivity spectra within the framework of the MIGRATION concept.

In the theory proposed by Austin and Mott,[3,15] the conduction process in TM oxide glasses occurs by phonon-assisted hopping of small polarons between nearest localized states. In this model, the temperature dependence of DC conductivity is given by the following expression:

$$\sigma_{DC} = \frac{\nu_{ph} e^2 C(1-C)}{k_B T R} \exp(-2\alpha R)\, \exp(-W/k_B T) \qquad (2)$$

where ν_{ph} is the phonon frequency ($\approx 10^{13}$ Hz), e is the charge of electron, C is the fraction of metal ions in the lower oxidation state, k_B is the Boltzmann constant, T is the temperature, R is the average spacing between transition metal ions ($R = N^{-1/3}$), α is the tunneling factor and W is the activation energy for DC conduction. As shown in Fig. 3(b), all glasses display the linear temperature dependence of $\log(\sigma_{DC}T)$ *vs.* $1000/T$, and from the slopes the activation energy for DC conductivity, W, was determined, see Table 2. As expected, the compositional dependence

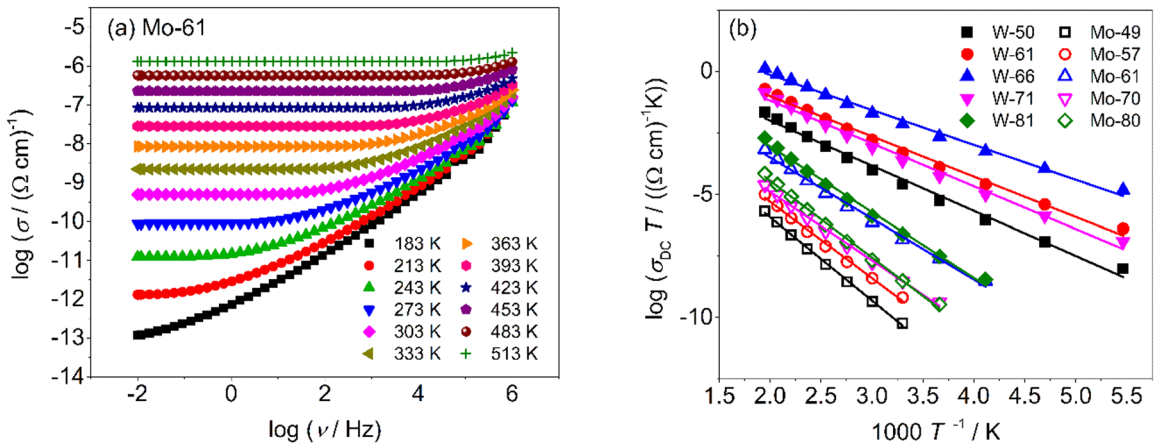

Fig. 3 (a) Conductivity spectra at different temperatures of the Mo-61 glass and (b) DC conductivity as a function of reciprocal temperature of phosphate glasses containing WO_3 (solid symbols) and MoO_3 (open symbols). The straight lines were obtained by linear regression. The error bars are at most of the order of the symbol size.

Table 2 Values of electrical parameters: DC conductivity, σ_{DC}, activation energy, W, the number of transition metal ions per volume, N, average spacing between transition metal ions, R, polaron radius, r_p, tunneling term, $\exp(-2\alpha R)$, and rate of the wave function decay, α, for glasses from $x$$WO_3$-$(100-x)P_2O_5$ and $x$$MoO_3$-$(100-x)P_2O_5$, x = 49–81 mol%, series

Glass	$\sigma_{DC}/(\Omega\ cm)^{-1}$ at 303 K	W (eV)	N (cm^{-3}) × 10^{21}	R (Å) = $N^{-1/3}$	r_p (Å)	$\exp(-2\alpha R)$	α ($Å^{-1}$)
W-50	8.53×10^{-8}	0.36	6.48	5.36	2.16	4.63×10^{-4}	0.72
W-61	1.66×10^{-6}	0.33	8.49	4.90	1.98	4.40×10^{-3}	0.55
W-66	2.40×10^{-5}	0.28	9.38	4.74	1.91	7.96×10^{-4}	0.75
W-71	7.74×10^{-7}	0.35	10.4	4.58	1.85	1.41×10^{-3}	0.72
W-81	8.04×10^{-10}	0.53	12.9	4.26	1.72	1.18×10^{-3}	0.79
Mo-49	1.94×10^{-13}	0.67	6.24	5.43	2.19	1.28×10^{-5}	1.04
Mo-57	2.13×10^{-12}	0.62	7.60	5.09	2.05	1.41×10^{-5}	1.10
Mo-61	4.96×10^{-10}	0.49	8.31	4.94	1.99	4.08×10^{-5}	1.02
Mo-70	9.84×10^{-12}	0.55	9.76	4.68	1.89	7.35×10^{-5}	1.02
Mo-80	1.02×10^{-11}	0.62	10.2	4.37	1.76	9.76×10^{-4}	0.79

of activation energy for glasses containing WO_3 and MoO_3 shows the opposite trend as does the DC conductivity. According to the small polaron hopping theory, the polaron is expected to be localized in the potential well from which the hopping process occurs in an adiabatic or a non-adiabatic way. In the adiabatic regime, the tunneling probability $\exp(-2\alpha R)$ is approximately 1 and negligible while in the non-adiabatic regime it is much less than 1, meaning that the chance of polaron tunneling between two potential wells is rather small. The tunneling term for all the glasses is calculated from the pre-exponential factor and is found to be far less than 1, see Table 2. Although these values are indeed larger by an order of magnitude in the binary tungsten phosphate glasses when compared to the molybdenum phosphate systems, they are nevertheless much less than one, and we believe that it does not lend to any evidence of an adiabatic character of the polaronic transport for the tungsten phosphate glasses as proposed by Murawski *et al.*[5] Thus, our analysis shows the non-adiabatic hopping process in glasses from both WO_3–P_2O_5 and MoO_3–P_2O_5 series, see Table 2. The values of the tunneling factor, α, average spacing between transition metal ions, R, and polaron radius, r_p, estimated from the expression proposed by Bogomolov and Mirilin,[33] $r_p = \frac{1}{2}\left(\frac{\pi}{6N}\right)^{1/3}$, are also reported in Table 2. The values of the rate of the wave function decay, α, and the polaron radius, r_p, are in good agreement with similar polaron conducting glasses.[4,15,16,18]

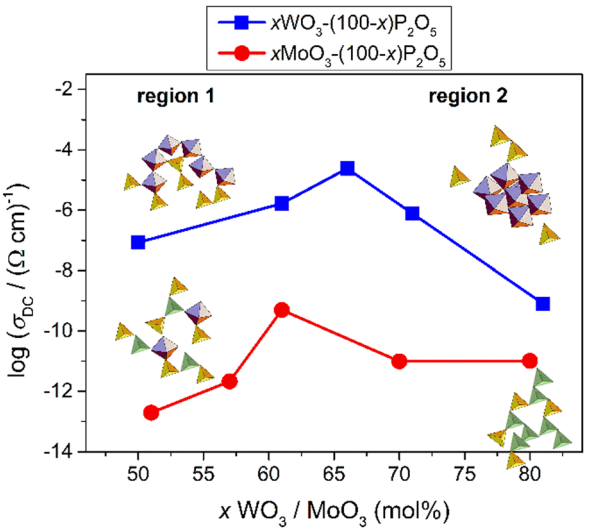

Fig. 4 Compositional dependence of DC conductivity at 303 K for $x$$WO_3$-$(100-x)P_2O_5$ and $x$$MoO_3$-$(100-x)P_2O_5$, x = 49–81 mol% glass series. Region 1 includes glass compositions up to the conductivity maximum with the 2D interconnection of TM units, whereas region 2 corresponds to the glass compositions above the conductivity maximum where the 3D interconnection of TM units occurs. The lines are drawn as a guide to the eye.

3.3.2. What does the network structure got to do with the transport of polarons? The compositional dependence of DC conductivity, σ_{DC}, at 303 K shown in Fig. 4 exhibits two remarkable effects upon the addition of MoO_3 and WO_3. The first one is related to the significantly higher conductivity of tungsten glasses throughout the entire range of compositions and the second one is ascribed to the non-monotonic trend of DC conductivity with maxima at 61 mol% of MoO_3 and 66 mol% of WO_3.

In order to explain the observed conductivity trends, several parameters need to be discussed. According to the classical understanding of the polaronic transport in oxide glasses, one of the most important factors for conductivity is the fraction of reduced TM ions (TM^{5+}/TM_{tot}). The increase of this fraction usually causes an increase in polaronic conductivity due to the increase in the number of TM^{5+}–TM^{6+} ion pairs through which the electron transfer occurs. Our results, however, contradict this hypothesis. For one, the fraction of W^{5+}/W_{tot} is $\lesssim$1.9% throughout the entire series but the DC conductivity varies largely. On the other hand, with the addition of MoO_3 from 49% to 61%, the Mo^{5+}/Mo_{tot} ratio decreases while the DC conductivity simultaneously increases, see Table 1. Even if we take into account the increase in the MoO_3 content and calculate the number density of Mo^{5+} ions we see that this value changes from $\approx 1.7 \times 10^{21}$ cm^{-3} to $\approx 1.3 \times 10^{21}$ cm^{-3} as the amount of MoO_3 increases to 61%, which, again, cannot explain the observed increase in conductivity. Secondly, if we compare the two glass systems, tungsten glasses exhibit significantly higher DC conductivity than their molybdenum counterparts despite a significantly lower W^{5+}/W_{tot} ratio. This difference is especially pronounced at the

lowest TMO content of about 50–60 mol%, where the greatest difference between W^{5+}/W_{tot} and Mo^{5+}/Mo_{tot} is observed. A similar difference in conductivity between these two glass systems was reported in previous studies; however, therein, glasses were investigated in a relatively narrow range of compositions.[4,6,23] For instance, Sayer and Mansingh[4] reported approximately five orders of magnitude higher electrical conductivity of $50WO_3$–$50P_2O_5$ than that of the $50MoO_3$–$50P_2O_5$ glass and our recent study[23] showed a similar conductivity difference for $60WO_3$–$40P_2O_5$ (4.26×10^{-6} $(\Omega\ cm)^{-1}$) and $60MoO_3$–$40P_2O_5$ (2.76×10^{-11} $(\Omega\ cm)^{-1}$) glasses. In these studies, the higher electrical conductivity of tungsten glasses in comparison to molybdenum analogues was ascribed to the clustering of tungstate units that ease the polaronic transport; *i.e.* the higher number of facilitating W–O–W bonds in comparison to the higher number of inhibiting Mo–O–P bonds in molybdenum glasses. In our present study, we show that the higher conductivity of tungsten glasses is evident throughout the wide compositional range, *x*(TMO) ranging from 50 to 80 mol%, and that, indeed, this difference can be related to the glass structure. In fact, as per the analysis in Section 3.2.1., it emerges that all tungsten containing glasses are characterized by a high tendency of WO_6 units to mutually connect and form W–O–W–O–W bonds that gradually start to dominate the glass network as the amount of WO_3 increases. On the other hand, in the molybdenum glasses, MoO_6 octahedra and MoO_4 tetrahedra are interconnected with the phosphate units forming a mixed phosphate–molybdate glass network. From this, it is reasonable to assume that the network composed of tungstate clusters provides more conductive pathways for polarons *via* W–O–W bonds than the mixed phosphate–molybdate network with preferred Mo–O–P bonding. Therefore, the increase in the polaronic conductivity of glasses containing up to 66 mol% of WO_3 and 61 mol% of MoO_3 (marked as region I in Fig. 4), as well as the difference between the two series, is directly related to the increase in the number of W–O–W and Mo–O–Mo bonds with increasing TMO, as well as a generally higher fraction of W–O–W bonds in comparison to Mo–O–Mo bonds (see Fig. 1).

However, although the formation of the fast polaron transport pathways *via* bridging TM–O–TM bonds explains well the trends up to the conductivity maximum, it fails to explain the decrease in conductivity with the further addition of both oxides. In particular, it is interesting to observe that the decrease in conductivity is especially strong in tungsten glasses for which the formation of W–O–W bonds is extremely favored. Again, this result is in disagreement with the general idea that clustering of TM units has a facilitating effect on polaron transport. So, the main question to be answered is, what is the cause of the observed decrease in conductivity at high amounts of WO_3 and MoO_3? From the Raman spectra shown in Fig. 1(a), we observe that above 66 mol% of WO_3, WO_6 octahedra form a three-dimensional network by consuming oxygen atoms for linking and hence causing a strong decrease in the number of terminal oxygen bonds (see upper panels in Fig. 1). Such formation of WO_6 clusters with a small number of terminal oxygens results in a rigid tungstate network which seems to be unfavorable for the structural rearrangement involved in polaron formation and hence its conductivity. This is especially evident in the W-81 glass for which the polaronic conductivity shows the strongest decrease along with the strongest decrease in the intensity of the Raman band corresponding to the terminal oxygen atoms, compare Fig. 1(a) and 4. This further indicates that the key factor that governs the polaronic transport in these glasses is the way in which the tungstate units interconnect, or more precisely the interplay between the number of bridging and terminal oxygen bonds which defines the flexibility of the tungstate network. Accordingly, when the former bonds start to overpower the latter, the network becomes rigid and the conductivity gets hindered. A similar finding on the importance of the flexibility of the bonds involved in polaronic transport was recently reported for crystalline V_2O_5.[34] Based on the DFT+U calculations, the authors showed that the least favourable polaron migration pathway is through the stiff 3-coordinated oxygen atom connected between vanadium centres that results in a distorted transition state structure with high energy. In contrast, bridging V–O–V bonds appear to be favorable for polaron migration even though their hopping distance is quite large. The reason for this is the higher flexibility of bridging oxygen atoms which causes a less constrained transition state structure and a lower transition state energy. Furthermore, our most recent study on binary V_2O_5–P_2O_5 glasses exhibits an almost linear increase in the polaronic conductivity, even up to 90 mol% of V_2O_5, followed by a gradual increase in the intensity of bridging V–O–V bonds but with the retained high intensity of terminal V–O bonds over the entire compositional range.[35] These findings support our conclusion that for fast polaron transport it is crucial to have TM–O–TM bonding; however, once the clustering of TM units starts to occur three-dimensional with a significant loss of flexible terminal oxygen bonds, polaronic transport gets hampered.

Similar correlations can also be made for molybdenum glasses in which the polaronic conductivity drops above 61 mol% of MoO_3 (see region II in Fig. 4). In this system too, the Raman spectra show that the three-dimensional networking of molybdenum units takes place above 61 mol% of MoO_3 and eventually rigid oxygen bonds dominate causing a decrease in polaronic conductivity. However, here, the decrease, while significant for Mo-70, does not decrease further for Mo-80. The network connectivity offered by MoO_4 tetrahedra *vis-a-vis* the significant loss of flexible terminal oxygen bonds has an obvious role in this implying that the coordination of TM ions, *i.e.* octahedral *vs.* tetrahedral, also plays a role in the ease of charge conduction in these glasses. In the next step, we aim to shed some light on these trends with our analysis of the conductivity and permittivity spectra using the MIGRATION concept.

3.3.3. Insights into the structure–conductivity correlations on modelling the frequency-dependent conductivity and permittivity using the MIGRATION concept. A scaled model spectrum from the MIGRATION concept is generated for a particular set of values of the three model parameters, K, B & $N(\infty)$, described earlier. The very nature of the model and the formulation makes this model spectrum satisfy the time-temperature superposition principle (TTS). Hence, it is plotted

in a scaled representation as $\log(\sigma_s(\omega_s))$ *vs.* $\log(\omega_s)$, where $\sigma_s(\omega_s) = \frac{\sigma(\omega_s)}{\sigma_{DC}}$, with $\omega_s = \frac{\omega}{\omega_O} = \frac{\nu}{\nu_O}$. Using σ_{DC} determined from the experiment, the suitable model spectrum is chosen on shifting the experimental isotherm on the scaled *x*-axis by $\log(\nu_o)$, which is defined as the onset frequency of conductivity dispersion for that temperature, such that the shape and form of the experimental isotherm match that of the model isotherm. Here, the crucial model parameter describing the shape of the isotherm around the onset of conductivity dispersion is *K*. Normally for ionic glasses, *B* can be chosen arbitrarily large and $N(\infty)$ can be set to zero for this step. However, in polaronic glasses, as in mixed former ionic glasses,[36] rather a small value of *B* is needed to describe the shape of the permittivity isotherm, and a non-zero value of $N(\infty)$ is additionally needed to model the gradual onset of conductivity dispersion at lower frequencies of the isotherm. The model permittivity spectrum is plotted as $\varepsilon_s(\omega_s)$ *vs.* $\log(\omega_s)$, and is defined as $\varepsilon_s(\omega_s) = \frac{\varepsilon_0\omega_O}{\sigma_{DC}} \cdot (\varepsilon(\omega_s) - \varepsilon(\infty))$. In polaronic glasses, the scaled permittivity isotherm exhibits a reasonably well-defined low-frequency plateau, $\varepsilon_s(0)$. Note that $\varepsilon(\infty)$ is the permittivity due to faster electronic relaxation processes and is not related to the slower relaxation processes connected with polaronic hopping. In Fig. 5, we plot conductivity and permittivity isotherms in the scaled representation for W-66 and Mo-61 glasses, superimposed on the model curves that best describe the experimental spectra. The experimental conductivity spectra of the Mo-61 glass are shown in Fig. 3a, whereas its permittivity spectra as well as the conductivity and permittivity spectra of the W-66 glass are shown in Fig. S1 of the ESI.†

Table 3 Values of model parameters of the MIGRATION concept for glasses from xWO$_3$-(100−x)P$_2$O$_5$ and xMoO$_3$-(100−x)P$_2$O$_5$, x = 50–80 mol% series

Glass	*K*	*B*	$N(\infty)$	ε_s (0)	$\langle r_{loc}^2(\infty)\rangle^{0.5}$ in Å
W-50	2.0	12	0.12	2.67	1.47 ± 0.06
W-61	1.9	12	0.09	2.81	1.27 ± 0.05
W-66	1.9	12	0.11	2.66	1.21 ± 0.03
W-71	2.0	12	0.02	4.31	1.53 ± 0.02
Mo-57	2.2	12	0.02	5.25	2.08 ± 0.07
Mo-61	2.1	12	0.08	3.15	1.11 ± 0.03
Mo-70	2.2	12	0.13	2.73	1.06 ± 0.05
Mo-80	2.2	12	0.10	3.03	0.92 ± 0.03

In Table 3, we present the parameters of the model spectra used for modelling the conductivity and permittivity spectra of glasses from the xWO$_3$-(100−x)P$_2$O$_5$ and xMoO$_3$-(100−x)P$_2$O$_5$ series. To recall, the W-81 glass was excluded from analysis due to partial crystallization, and Mo-49 due to the lack of a good permittivity plateau in experimental isotherms. In considering the observed changes in the parameter *K*, two comments are in order. Firstly, the variation in *K* shows a neat inverse correlation to DC conductivity for both systems. Secondly, the absolute values of *K* for glasses containing WO_3 are lower (K = 1.9 and 2.0) than those for glasses containing MoO_3 (K = 2.1 and 2.2) which is in agreement with the trends exhibited for the values of DC conductivity in these glasses, see Fig. 4. From the body of spectra which have been so far modelled using the MIGRATION concept, it has been found that for the majority of the single-alkali ionic glasses be it borate, silicate or phosphate glasses or in mixed glass formers systems, the parameter *K* has

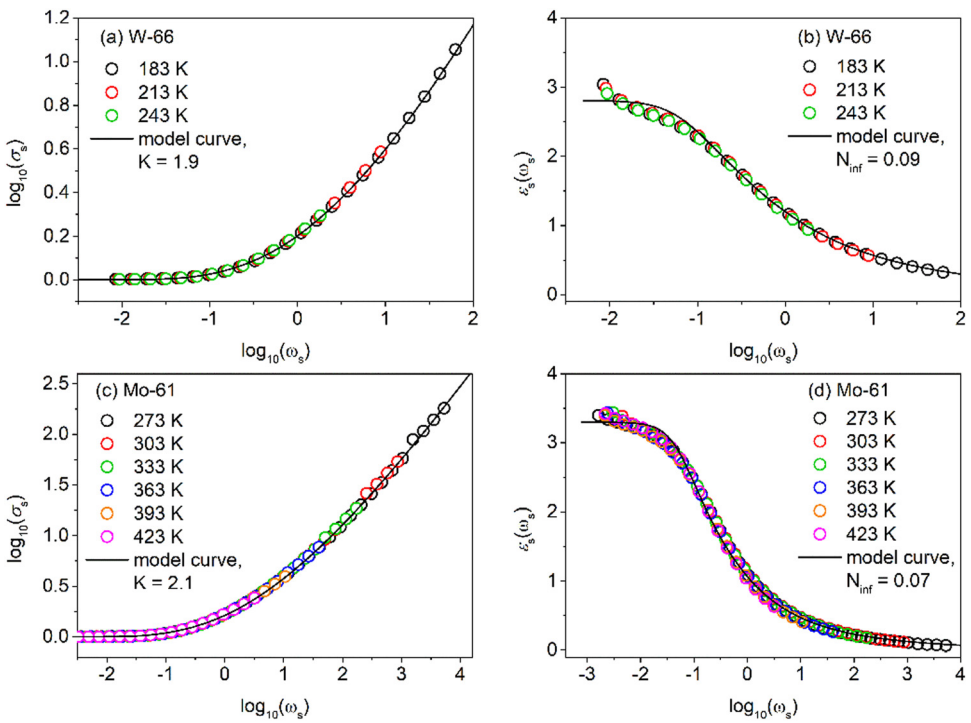

Fig. 5 Scaled experimental (a and c) conductivity and (b and d) permittivity spectra of W-66 and Mo-61 glasses superimposed on corresponding model curves with B = 12.

a value of 2.0.[25,26,36] In ionic glasses, values of $K > 2.0$ could be correlated to either a lower connectivity of conductivity pathways or a lower number density of the charge carriers.[37–39] On the other hand, for polaronic iron phosphate-based glasses, the value of K was found to be 1.9, indicating an earlier onset of long-range charge transport in contrast to ionic glasses.[9] It is to be noted that although the K parameter has been found to have values from 1 to 3 in the spectra of materials modelled so far, a difference of 0.1 on either side of $K = 2.0$ is significant. Thus, one of the factors responsible for a much higher value of σ_{DC} in the W-66 glass as compared to that of Mo-61, see Fig. 4, is the ease of the transport of polarons in the former. Also, it is important to note that although the value for the two glasses W-61 and W-66 is K =1.9 as in the polaronic iron phosphate glasses,[9] the factors responsible for it are different. In the latter systems, the fraction of the reduced iron ions is correlated directly to σ_{DC}, see Fig. 8 in ref. 9, while the phosphate glass network structure remains very similar. This is not true for phosphate glasses containing tungsten and molybdenum oxides studied here. In our current study, it is evident that the polaron conductivity is driven by the structural features of the glass such as the network connectivity of different structural units (see Fig. 1 and discussions following it) and is not correlated to the TM^{5+} fraction. Therefore, we infer that an increase from $K = 2.1$ for Mo-61 glasses to $K = 2.2$ for all other MoO_3 contents is indicative of lesser available pathways for the polaron transport in the glass network in the latter samples. On the other hand, the value of K decreasing from 2.0 for W-50 and W-71 glasses to 1.9 for W-61 and W-66 samples suggests that the network connectivity is less important than the faster local relaxations which implies shallow potential wells and hence faster polaronic transport. Indeed, from the structural results based on the analysis of Raman and ^{31}P MAS-NMR spectra, we can infer that one main advantage of the clustering of tungstate units is that they could allow for fast local relaxations. And a larger value of σ_{DC} as well as this small value of $K = 1.9$ allows us to put forth a picture of *tissue connectivity*, where the polaron transport within the nodules composed of two-dimensionally connected tungsten units is fast and there is a conducting pathway to the next cluster.

In the right-hand side panels of Fig. 5, we present the scaled permittivity spectra of W-66 and Mo-61 samples with the corresponding master spectrum (the similar representation of the modelled scaled permittivity spectrum for other glasses is shown in Fig. S2 of the ESI†). Here, a suitable value of the parameter, $N(\infty)$, helps us to find the plateau value of $\varepsilon_s(0)$. The value of B could be ascertained by modelling the permittivity spectrum and is found to be rather small, implying that for the lowest measured temperature, conductivity dispersion cannot be more than 5.2 decades on the logarithmic scale. This further implies that, for instance, for the Mo-61 glass at the lowest temperature (namely 183 K), the high-frequency conductivity plateau would lie just close to a few MHz. This result in itself is sensational, since polaronic glasses have not been measured at higher frequencies and, based on this inference from modelling, it could imply that any further dispersion one would observe in conductivity at higher frequencies may not correspond to processes contributing to translational charge transport, but rather to localized relaxation processes of the oxide network. We also observe that B = 12 fits the permittivity spectrum of the highly conductive W-66 glass, although even at 183 K, due to the higher value of DC conductivity, the tail of $\varepsilon(\infty)$ attaining a zero value is not yet observed in the experimental frequency range. A perusal of Table 3 reveals that the value of $\varepsilon_s(0)$ changes from 5.25 to 2.73 for the glasses containing MoO_3 while it is around 2.7–2.8 for glasses containing WO_3, except for W-71.

In Table 3, we additionally quantify the length scale of the localized polaronic hops, $\langle r_{loc}^2(\infty)\rangle^{0.5}$ for each composition using the relationship (3):

$$r_{loc}^2(\infty) = \frac{6k_B\sigma_{DC}T}{N_v q^2}\cdot\frac{\varepsilon_S(0)}{\omega_0} \quad (3)$$

Note that by definition this quantity is independent of temperature if $\omega_0 \propto \sigma_{DC}T$ is valid. This further implies that the Summerfield scaling of conductivity spectra is valid. The results of the model-free investigation of the scaling properties of these glasses using the Summerfield and Sidebottom procedure are given in the Section 4 of the ESI.† As can be seen from these results for all glasses modelled here, except for Mo-57, the Summerfield scaling procedure yields a conductivity master-curve. However, for Mo-57, since we showed that the Sidebottom scaling is valid, and since the shape parameter K also remains the same with temperature, the length scale of the localized polaronic hops is also temperature-independent. Also note that, unlike in ref. 9, where we used $N_v = C{\cdot}N$, and the experimental $\langle\Delta\varepsilon{\cdot}T\rangle$ to calculate $\langle r_{loc}^2(\infty)\rangle$, here we define N_v to be the total content of TM ions in the glass, N, and use the model value of $\varepsilon_s(0)$ to calculate $\langle r_{loc}^2(\infty)\rangle$. This choice of N_v is justified based on various inferences made so far on the structural results and the exhibited trend of σ_{DC} and parameter K with the glass composition which led us to conclude that structural aspects influence polaron transport and the role of C is minimal. The square root of the quantity $\langle r_{loc}^2(\infty)\rangle$ which can be viewed as a kind of dynamic polaron radius[9] is found here to be smaller than r_p (compare their values in Tables 2 and 3) unlike in iron phosphate glasses. One strong reason could be that the deformation of the local potential wells is smaller (and shallower as proposed earlier). Furthermore, we note that the values are lower for those glass compositions with higher σ_{DC} and this seems to indicate that these values of the dynamic polaron radius correlate with the trend in σ_{DC}.

In considering the parameters in Table 3, it is interesting to note that in these glasses despite a steady increase in N as a function of the TM oxide content, see Table 2, all dynamic values of polaron transport, parameter K, $\langle r_{loc}^2(\infty)\rangle^{0.5}$ and $\varepsilon_s(0)$ mirror each other. This confirms the inferences from a detailed structural analysis that the dynamics of polaron transport in these glasses is guided by the interconnectivity of structural units and hence the formation of conduction pathways for the polarons. Two features that are worthy of comments are (i) for the glasses containing MoO_3, there is a strong decrease of $\varepsilon_s(0)$,

which is also reflected in the trend shown by $\langle r_{loc}^2(\infty)\rangle^{0.5}$ and (ii) an increase in $\varepsilon_s(0)$ for the W-71 glass in the series containing WO_3. We recall that the Mo-57 glass exhibits the lowest conductivity among the four compositions that could be modelled for this series. As discussed earlier, the number of Mo–O–Mo bonds increases with the increase in the MoO_3 content which explains the ease of polaron conductivity due to better network connectivity. In contrast, for the W-71 glass, the absence of terminal oxygen bonds means the three-dimensional networking of WO_6 octahedra and hence increased charge stored in W–O–W–O–W bridges in clusters, which is reflected both by an increase in $\varepsilon_s(0)$, as well as in parameter K and $\langle r_{loc}^2(\infty)\rangle^{0.5}$.

One last feature worth mentioning is that unlike in the mixed glass former glasses with ions as charge carriers,[36] where $\langle r_{loc}^2(\infty)\rangle^{0.5}$ features the same compositional dependence as σ_{DC}; here, the typical polaronic hopping length is inversely correlated with σ_{DC}, compare Fig. 3 and Table 3, similarly as in polaronic iron phosphate glasses.[9,40] This brings to focus the fact that polaronic conductivity has distinctive features that distinguish them from ionic charge carriers. As it is the transport of charge that propagates in the form of polaronic hops, whereas in ionic glasses, there is a spatial propagation of the charged species. Correspondingly, the value of $\langle r_{loc}^2(\infty)\rangle^{0.5}$ is a physical quantity there, whereas it is a characterization of the spatial extent of the local dipolar disturbance field in polaronic glasses.

4. Conclusions

This study reports on the nature of polaronic conductivity in binary phosphate glasses containing WO_3 and MoO_3 in a wide compositional rage: $x$$WO_3$-(100−$x$)$P_2O_5$ and $x$$MoO_3$-(100−$x$)$P_2O_5$, x = 49–81 mol%. The results show that the parameters of the polaronic transport cannot be correlated to the fraction of reduced tungsten and molybdenum ions and the overall amount of WO_3 and MoO_3, which are the factors that are generally acknowledged to have the most important role in electrical processes in glasses. In contrast, our detailed structural and electrical studies using Raman, ^{31}P MAS-NMR, ESR and impedance spectroscopies, as well as numerical modelling of the conductivity and permittivity spectra using the MIGRATION concept revealed that the polaronic conductivity in these glasses is entirely governed by the structural characteristics of the glass network. Firstly, a significantly higher conductivity (nearly six orders of magnitude) of glasses containing WO_3 in comparison to their MoO_3 counterparts results from the high tendency of WO_6 units to aggregate by forming W–O–W–O–W bridges which act as easy conduction pathways. Molybdenum units, MoO_4 and MoO_6, on the other hand, tend to uniformly incorporate into the phosphate network by forming P–O–Mo bonds that hinder the ease of polaron hops. Secondly, the non-monotonic trend of polaronic conductivity as a function of glass composition, showing maxima at 61 mol% of MoO_3 and 66 mol% of WO_3, indicates that the key factor that governs the polaronic transport in these glasses is the manner in which the tungstate and molybdenum units interconnect mutually. While the two-dimensional interconnection of these units has a positive effect on the dynamics of polarons by providing fast conduction pathways, the three-dimensional linking negatively affects the polaron transport due to a decrease in the number of terminal TM–O bonds which are important for the formation and transport of polarons. To state it simply, the clustering of transition metal units in oxide glasses does not facilitate the polaronic conductivity *per se*; it is the manner in which these units are connected that governs the conduction process.

Conflicts of interest

There are no conflicts to declare.

Acknowledgements

This work is supported by the Croatian Science Foundation, POLAR-ION-GLASS project IP-2018-01-5425. P. M. and L. K. are grateful for the financial support from the project no. 18-01976S of the Grant Agency of the Czech Republic.

References

1 E. P. Denton, H. Rawson and J. E. Stanworth, *Nature*, 1945, **173**, 1030–1032.
2 N. F. Mott, *J. Non-Cryst. Solids*, 1968, **1**, 1–17.
3 I. G. Austin and N. F. Mott, *Adv. Phys.*, 1969, **18**(71), 41–102.
4 M. Sayer and A. Mansingh, *Phys. Rev. B: Solid State*, 1972, **6**(12), 4629–4643.
5 L. Murawski, C. H. Chung and J. D. Mackenzie, *J. Non-Cryst. Solids*, 1979, **32**, 91–104.
6 N. Chopra, V. Gupta, A. Mansingh and G. K. Chadha, *Philos. Mag. B*, 1997, **75**, 249–259.
7 C. H. Chung and J. D. Mackenzie, *J. Non-Cryst. Solids*, 1980, **42**, 357–370.
8 A. Šantić and A. Moguš-Milanković, *Croat. Chem. Acta*, 2012, **85**(3), 245–254.
9 A. Šantić, R. D. Banhatti, L. Pavić, H. Ertap, M. Yüksek, M. Karabulut and A. Moguš-Milanković, *Phys. Chem. Chem. Phys.*, 2017, **19**, 3999–4009.
10 X. Fang, C. S. Ray, A. Moguš-Milanković and D. E. Day, *J. Non-Cryst. Solids*, 2001, **283**, 162–172.
11 C. Mercier, G. Palavit, L. Montagne and C. Follet-Houttemane, *C. R. Chimie*, 2002, **5**, 693–703.
12 G. Poirier, F. S. Ottoboni, F. C. Cassanjes, A. Remonte, Y. Messaddeq and S. J. L. Ribeiro, *J. Phys. Chem. B*, 2008, **112**, 4481–4487.
13 M. Ataalla, A. S. Afify, M. Hassan, M. Abdallah, M. Milanova, H. Y. Aboul-Enein and A. Mohamed, *J. Non-Cryst. Solids*, 2018, **491**, 43–54.
14 A. Mansingh, J. K. Vaid and R. P. Tandon, *J. Phys. C: Solids State Phys.*, 1976, **9**, 1809–1817.
15 A. Mansingh, J. K. Vaid and R. P. Tandon, *J. Phys. C: Solids State Phys.*, 1977, **10**, 4061–4066.

16 A. Mansingh, A. Dhawan, R. P. Tandon and J. K. Vaid, *J. Non-Cryst. Solids*, 1978, **27**, 309–318.
17 A. Mansingh, R. P. Tandon and J. K. Vaid, *Phys. Rev. B: Condens. Matter Mater. Phys.*, 1980, **21**(10), 4829–4839.
18 M. H. Hekmat-Shoar, C. A. Hogarth and G. R. Moridi, *J. Mater. Sci.*, 1985, **20**, 889–894.
19 A. M. Al-Shukri, G. D. Khattak and M. A. Salim, *J. Mater. Sci.*, 2000, **35**, 123–126.
20 S. V. Pershina, S. N. Shkerin and A. S. Tolkacheva, *Int. J. Energy Res.*, 2019, 1–7.
21 S. V. Pershina, *Russ. J. Appl. Chem.*, 2019, **92**(4), 482–489.
22 J. Nikolić, L. Pavić, A. Šantić, P. Mošner, L. Koudelka, D. Pajić and A. Moguš-Milanković, *J. Am. Ceram. Soc.*, 2018, **101**, 1221–1235.
23 L. Pavić, A. Šantić, J. Nikolić, P. Mošner, L. Koudelka, D. Pajić and A. Moguš-Milanković, *Electrochim. Acta*, 2018, **276**, 434–445.
24 K. Funke and R. D. Banhatti, *Solid State Ionics*, 2004, **169**, 1–8.
25 K. Funke and R. D. Banhatti, *Solid State Ionics*, 2006, **177**, 1551–1557.
26 R. D. Banhatti, C. Cramer, D. Zielniok, A. H. Jean Robertson and M. D. Ingram, *Z. Phys. Chemie*, 2009, **223**, 1201–1215.
27 L. Koudelka, J. Šubčík, P. Mošner, L. Montagne and L. Delevoye, *Phys. Chem. Glasses: Eur. J. Glass Sci. Technol. B*, 2012, **53**(3), 79–85.
28 J. Šubčík, L. Koudelka, P. Mošner, L. Montagne, G. Tricot, L. Delevoye and I. Gregora, *J. Non-Cryst. Solids*, 2010, **256**, 2509–2516.
29 D. R. Lide, *CRC Handbook of Chemistry and Physics*, CRC Press, Boca Raton, Florida, 2009, pp. 9–68.
30 C. Y. Kim and R. A. Condrate, *J. Phys. Chem. Solids*, 1984, **45**, 1213–1218.
31 S. H. Santagneli, C. C. de Araujo, W. Strojek, H. Eckert, G. Poirier, S. J. L. Ribeiro and Y. Messaddeq, *J. Phys. Chem. B*, 2007, **111**, 10109–10117.
32 M. Lahaye, B. Doumert, B. Revel, K. Ben Tayeb, H. Vezin and G. Tricot, *J. Phys. Chem. C*, 2015, **119**, 17288–17297.
33 V. N. Bogomolov and D. N. Mirlin, *Phys. Stat. Solidi B*, 1968, **27**, 443–453.
34 P. Watthaisong, S. Jungthawan, P. Hirunsit and S. Suthirakun, *RSC Adv.*, 2019, **9**, 19483–19494.
35 M. Razum, L. Pavić, D. Pajić, J. Pisk, T. Čižmar and A. Šantić, Novel insights into the mechanism of polaronic conduction in binary V_2O_5-P_2O_5 glasses, in preparation.
36 K. Sklepić, R. D. Banhatti, G. Tricot, P. Mošner, L. Koudelka and A. Moguš-Milanković, *J. Phys. Chem. C*, 2017, **121**, 17641–17657.
37 R. D. Banhatti and K. Funke, *Solid State Ionics*, 2004, **175**, 661–663.
38 C. Cramer, S. Brückner, Y. Gao and K. Funke, *Phys. Chem. Chem. Phys.*, 2002, **4**, 3214–3218.
39 K. Funke, R. D. Banhatti, S. Brückner, C. Cramer, C. Krieger, A. Mandanici, C. Martiny and I. Ross, *Phys. Chem. Chem. Phys.*, 2002, **4**, 3155–3167.
40 L. Pavić, S. Fazinić, H. Ertap, M. Karabulut, A. Moguš-Milanković and A. Šantić, *Materials*, 2020, **13**(2505), 1–15.